IL33-regulated NPM1 promotes fibroblast-to-myofibroblast transition via ERK/AP-1 signaling in silica-induced pulmonary fibrosis

Yue Wang
Nanjing Medical University
Demin Cheng
Nanjing Medical University
Ziwei Li
Nanjing Medical University
Wenqing Sun
Nanjing Medical University
Siyun Zhou
Nanjing Medical University
Lan Peng
Nanjing Medical University
Haojie Xiong
Nanjing Medical University
Xinying Jia
Nanjing Medical University
Wei Li
Nanjing Medical University
Lei Han
Jiangsu Provincial Center for Disease Control and Prevention
Yi Liu
Nanjing Medical University
Chunhui Ni (chninjmu@126.com)
Nanjing Medical University

Research Article

Keywords: IL33, NPM1, ERK/AP-1 signaling, pulmonary fibrosis, silicosis

Posted Date: October 12th, 2022

DOI: https://doi.org/10.21203/rs.3.rs-1982434/v2

Abstract

Background: Silicosis is a global occupational lung disease caused by the accumulation of silica dust. There is a lack of effective clinical drugs, and the pathogenic mechanisms remain obscure. Interleukin 33 (IL33), a pleiotropic cytokine, could promote wound healing and tissue repair via the receptor ST2. However, the mechanisms by which IL33 involves in silicosis progression need further exploration.

Results: Here, we demonstrated that the IL33 levels in the lung sections were significantly overexpressed after bleomycin (BLM) and silica treatment. ChIP assay, knockdown and reverse experiments were performed in lung fibroblasts to prove gene interaction following exogenous IL33 treatment or co-cultured with silica-treated lung epithelial cells. Mechanistically, we illustrated that silica-stimulated lung epithelial cells secreted IL33 and further promoted the activation, proliferation, and migration of pulmonary fibroblasts by activating the ERK/AP-1/NPM1 signaling pathway in vitro. Also, Treatment with NPM1 siRNA-loaded liposomes markedly protected mice from silica-induced pulmonary fibrosis in vivo.

Conclusions: In this study, we identified that NPM1 could involve in the progression of silicosis, which was regulated by IL33/ERK/AP-1 signaling. And treatment methods targeting this pathway may provide new anti-fibrotic clues in pulmonary fibrosis.

Background

Silicosis is an ancient and incurable interstitial lung disease caused by inhaling respirable crystalline silica (RCS) dust mainly in the workplace, leading to persistent inflammation, irreversible fibrosis in the lungs, and eventually fatal respiratory failure [1]. Millions of workers in various industries are at risk of developing silicosis worldwide. Although preventive measures have been implemented for many decades, the prevalence rate of silicosis is still increasing in recent decades, especially in developing countries including China and India [2]. Apart from the widespread prevalence in low- and middle-income countries, the worrying increase in silicosis cases occurred in developed countries such as the USA, Australia, and Spain recently [3]. As a surgical treatment method, lung transplantation could cure silicosis. However, the condition is almost always progressive and devastating, and no specific drug treatment has been proven so far. Therefore, exploration of the complex pathogenesis and the new therapy discovery for silicosis should be highlighted.

According to the current studies, the main pathological mechanisms, including the recruitment of inflammatory cells, epithelial injury, and aberrant fibroblasts transition, are reported to contribute to the progress of silicosis [4, 5]. As a crucial part of pulmonary fibrosis, activated fibroblasts trans-differentiate into myofibroblasts (FMT) and secrete excessive extracellular matrix (ECM). The FMT progress is triggered by lung epithelial and immune cells secreted biological mediators, such as interleukin (IL) family, transforming growth factor-β (TGF-β), platelet-derived growth factor (PDGF), and connective tissue growth factor (CTGF) [6, 7]. Then resident fibroblasts in the lung lesion transform into α-smooth muscle

actin positive (α-SMA^{+}) myofibroblasts coupled with a hypersecretion phenotype, which produces amounts of ECM proteins, such as collagens, elastin, and fibronectin [8, 9].

Interleukin 33 (IL33), a newly discovered member of the interleukin 1 (IL-1) cytokine family, is a crucial regulator of the inflammatory and immune process [10]. In the normal physiological environment, human IL33 is constitutively expressed and stored in the nucleus of endothelial and epithelial cells. Besides, IL33 could be released as an alarmin upon the inflammatory response, biomechanical stress, or necrotic cell death [11]. IL33 plays an integral role in lung homeostasis through its actions in wound repair, fibrosis, and remodeling processes [12]. A number of previous studies have documented that IL33 can bind to and signal through its receptor ST2, an orphan receptor of the IL-1R family, to induce the activation of downstream signaling pathways, ultimately leading to the production of several pro-inflammatory factors and growth factors [13]. Furthermore, IL33 mRNA and protein levels have been shown to be significantly increased in the bronchoalveolar lavage (BAL) fluids of patients with IPF and systemic sclerosis (SSc)-related fibrosis [14]. Although several lines of evidence demonstrate that there is a potential role of IL33/ST2 in fibroblast activation and tissue remodeling, there is still room for better understanding.

Among the kinases activated by IL33, the ERK signaling pathway has been thoroughly studied, which has influenced diverse cellular events, including cell growth, proliferation, differentiation, migration, survival, and apoptosis [15]. Activated ERK1/2 not only regulates the target substrates in the cytoplasm, also translocates into the nucleus and phosphorylates various transcription factors to regulate the expression of genes. Importantly, recent studies have revealed that ERK signaling pathway participates in the formation and development of silicosis [16]. Given that IL33/ST2 signaling potentially regulates fibroblast to myofibroblast transition, we hypothesized that IL33/ERK was involved in the pathogenesis of silicosis via ST2. Nucleophosmin (NPM1), also known as B23, is a major nucleolar protein with nucleocytoplasmic shuttling characteristics [17]. It is proposed that NPM1 serves multiple functions in cellular processes. NPM1 has been shown to be regulated in the signaling pathway involving MAPKs/ERKs and c-Myc [18]. Moreover, the induction of transcriptional regulator c-Jun, an activator protein-1 (AP-1) transcription factor, which can is regulated by the ERK signaling, upregulated the transcriptional level of NPM1 [19, 20]. Although few reports have tried to address the regulation of NPM1 expression, NPM1 could be reasonably speculated to be involved in fibrosis progression via ERK signaling activation in silicosis.

To test the possibility of this hypothesis, both silica- and BLM-induced mouse pulmonary fibrosis models were used. Also, the gain or loss of function studies were performed in vitro. Collectively, these data identified that NPM1 regulates the FMT process as a main downstream target of IL33 signaling. Further therapy targeting NPM1 may exert anti-fibrotic potential in silicosis.

Results

1. IL33 is overexpressed in the silica- and BLM-induced pulmonary fibrosis models

To determine the role of IL33 in silicosis, we first established a silicosis mouse model induced by silica (Fig. 1A). And BLM-treated mice were also used as a well-established pulmonary fibrosis model (Additional file 1: Fig. S1A). H&E staining showed fibrotic remodeling characteristics by accumulating typical fibrotic nodules and abnormal alveolar structure in the silica and BLM group (Fig. 1B, and Additional file 1: Fig. S1B). Moreover, the collagen deposition levels observed by hydroxyproline assay in the lung tissues were aberrantly increased (Fig. 1C). Consistently, the markedly higher expression of fibrosis markers, including Fibronectin, Collagen I, and α-SMA, were detected in lung tissues after silica and BLM treatment (Fig. 1D, E, F, G and H, and Additional file 1: Fig. S1C). Then we further addressed the expression of IL33 in the lungs of fibrotic mice. Interestingly, under silica or BLM stimulation, the levels of IL33 in lung sections were significantly higher than those of control subjects (Fig. 1I and J, and Additional file 1: Fig. S1D).

2. Il33 Promotes The Fmt Process Of Pulmonary Fibroblasts Via Its Receptor St2

As IL33 was significantly elevated in pulmonary fibrosis, we determined whether IL33 modulates the activation of pulmonary fibroblasts. The primary mouse lung fibroblasts (PMLFs) and MRC-5 cells were stimulated with exogenous IL-33. After treatment of IL33, the markedly higher protein expression of Fibronectin, Collagen I, and α-SMA, markers of myofibroblasts, were detected in pulmonary fibroblasts in a dose-dependent manner (Fig. 2A and B). Since ST2 is the known receptor of IL-33, we then performed ST2 loss-of-function assays in PMLFs and MRC-5 following IL33 treatment. As expected, the expression of ST2 was efficiently silenced following ST2 siRNA transfection (Fig. 2C). Knockdown of ST2 blocked FMT in PMLFs and MRC-5 after IL33 induction (Fig. 2D and E). Consistent results were also obtained by fluorescence analysis of α-SMA expression (Fig. 2F). Additionally, we also investigated the impact of IL33 on the proliferation of pulmonary fibroblasts by CCK8 assay. Consistently, the silencing of ST2 expression reduced the remarkable expansion of fibroblasts induced by IL33 treatment (Fig. 2G and H). Furthermore, we estimated the migration ability of pulmonary fibroblasts by wound-healing assay. It showed that the migration ability of MRC-5 was increased in the presence of IL33, while suppressed following ST2 siRNA (Fig. 2I). Collectively, these results demonstrated that IL-33 promotes the activation of pulmonary fibroblasts via ST2.

3. Erk/ap-1 Cascade Involves In The Il33 Stimulated Fmt Process

Since the possibility was explored that IL33 induced pulmonary fibrosis through potentiating ERK/AP-1 signaling [14, 16], we first examined the expression of AP-1 in both BLM and silica-induced pulmonary fibrosis mice. Similar to previous research, it showed that the mRNA levels of AP-1 (c-Jun and c-fos) were

significantly increased after silica and BLM treatment (Fig. 3A and B, and Additional file 1: Fig. S2). We then examined if IL33 acts on pulmonary fibroblasts to induce the expression of AP-1. The results showed that treatment with IL33 induced AP-1 elevation in pulmonary fibroblasts in a dose-dependent manner (Fig. 3C, D, E and F). Then, the ST2 siRNA was used to further assess whether IL-33 could modulate the activation of the ERK/AP-1 pathway in fibroblasts. Western blot analysis demonstrated increased ERK and c-Jun phosphorylation levels in fibroblasts after culture with exogenous IL-33, and not surprisingly, ST2 siRNA abrogated IL33 induced ERK and c-Jun phosphorylation in PMLFs and MRC-5 cells (Fig. 3G and H). Consistently, the upregulation of c-Jun induced by IL33 was markedly reversed after the knockdown of ST2 in MRC-5, while c-Fos levels were unchanged (Fig. 3I, and Additional file 1: Fig. S3). To further determine whether AP-1 was involved in the activation of pulmonary fibroblasts induced by IL33, we performed c-Jun loss-of-function assays in PMLFs and MRC-5 following IL33 treatment. Knockdown of c-Jun demonstrated that fibroblast differentiation to myofibroblast was blocked after IL33 induction, which was accompanied by the low expression of myofibroblasts markers (Fig. 3J, K and L). Consistent results were also obtained by fluorescence analysis of α-SMA expression (Fig. 3M). Additionally, we investigated the impact of AP-1 on the proliferation of pulmonary fibroblasts by CCK8 assay. The silencing of c-Jun reduced the proliferation rate of fibroblasts induced by IL33 treatment (Fig. 3N and O). Also, the wound-healing assay showed that the migration ability of MRC-5 was increased in the presence of IL33, which was suppressed by c-Jun siRNA (Fig. 3P). Taken together, IL33 stimulates the activation, proliferation, and migration of pulmonary fibroblasts by activating the ERK/AP-1 pathway via ST2.

4. Il33 Regulated Erk/ap-1 Activates Npm1 In Pulmonary Fibroblasts

It's reported that AP-1 regulates the NPM1 gene in the context of cancer [21]. We examined the expression of NPM1 in pulmonary fibrosis mice. It showed that the mRNA levels of NPM1 were elevated after silica or BLM treatment (Fig. 4A, and Additional file 1: Fig. S4). Consistent results were also observed by lung sections fluorescence analysis of NPM1 (Fig. 4B). We then examined if IL33 could induce the NPM1 expression in fibroblasts. The results suggested that treatment with IL33 increased the expression of NPM1 in pulmonary fibroblasts in a dose-dependent manner (Fig. 4C and D). We further interrogated if ERK/AP-1 is responsible for the induction of NPM1 expression by IL33. It's found that c-Jun siRNA abolished IL33-induced NPM1 upregulation in PMLFs and MRC-5 cells (Fig. 4E, F and G). To further confirm these results, the c-Jun plasmid was used to enhance its expression in MRC-5 cells (Fig. 4H). The over-expressed c-Jun further increased NPM1 mRNA and protein levels in MRC-5 cells followed by IL33 stimulation (Fig. 4I and J). Morever, chromatin immunoprecipitation (ChIP) assays demonstrated the direct binding of c-Jun to NPM1 promoter region. And the binding was enhanced in IL33-activated fibroblasts (Fig. 4K). These data indicated that IL33 promotes AP-1 binding activity and its specific interaction with the NPM1 promoter.

To better understand the role of NPM1 in IL33-activated pulmonary fibroblasts, we performed NPM1 loss-of-function assays in PMLFs and MRC-5 following IL33 treatment. Knockdown of NPM1 showed that

FMT was eliminated in PMLFs and MRC-5 after IL33 induction, which was accompanied by the downregulated myofibroblasts markers (Fig. 5A and B). We also proved that NPM1 knockdown did not affect c-Jun expression (Fig. 5A and B), suggesting that NPM1 is activated downstream of the AP-1 signaling pathway. Fluorescence analysis of α-SMA also showed consistent results (Fig. 5C). Additionally, we also investigated the impact of NPM1 on the proliferation of pulmonary fibroblasts by EDU assay. Consistently, fewer EdU-positive cells were noted in NPM1 siRNA and IL33 treated PMLFs than in IL33-treated PMLFs (Fig. 5D). Furthermore, the migration ability of MRC-5 was increased in the presence of IL33 while suppressed following NPM1 siRNA treatment (Fig. 5E). Thus, NPM1 functioned as an important downstream target of IL33/ERK/AP1 signaling, which regulated the FMT progress of pulmonary fibroblasts.

5. Epithelial-derived Il33 Activates Pulmonary Fibroblasts By Potentiating The Erk1/ap-1/npm1 Pathway In Silicosis

IL33 may be released by damaged epithelial cells responding to noxious stimulants such as allergens, infectious pathogens, and other inhalational toxins, including cigarette smoke [22]. So we wondered if lung epithelial cells produce IL33 after silica treatment. It showed that the markedly higher secretion of IL33 was detected in silica-treated BEAS-2B epithelial cells and reached its peak in the 200 μg/mL treatment group (Fig. 6A and B). To prove the role of epithelial-derived IL33 in silicosis progression, silica-treated BEAS-2B cells were co-cultured with MRC-5 fibroblast cells. The silica-stimulated BEAS-2B cells led to activation of MRC-5 cells, while knockdown of IL33 in BEAS-2B cells or silenced ST2 in MRC-5 both attenuated the activation effects on MRC-5 cells (Fig. 6C and D). Therefore, we hypothesized that epithelium-derived IL33 might be involved in regulating the activation of pulmonary fibroblasts. We also found that MRC-5 cultured with silica-treated BEAS-2B cell supernatant could significantly promote the phosphorylation of ERK and c-Jun, and accompanied by the increased expression of NPM1; however, knockdown IL33 in BEAS-2B cells or silenced ST2 in MRC-5 attenuated the upregulation trends of ERK/AP-1 signaling in MRC-5 cells (Fig. 6E and F). Taken together, these findings indicated that epithelial cells could activate pulmonary fibroblasts by secreting IL33 in an ERK1/AP-1/NPM1 manner in silicosis.

6. Npm1 Liposomal-sirna Treatment Evokes An Anti-fibrotic Effect In The Silica-induced Pulmonary Fibrosis Model

Since NPM1 plays a critical role in fibroblasts' activation, proliferation and migration, we hypothesize that targeting NPM1 may provide a anti-fibrotic effect in silicosis. To test the possibility of the assumption, we constructed NPM1 siRNA-loaded liposomes. First, three siRNAs targeting mouse NPM1 were used to assess the knockdown efficiency and chose the most efficient one (2#) to generate the NPM1 siRNA-loaded liposomes(Fig. 7A and B). The successfully constructed liposomes (Additional file 1: Fig. S5) were prepared to address the biodistribution of the liposomes in vivo. After tail vein injection of the liposomes, mice were imaged by in vivo imaging system at different time points (0h, 24h, 48h). The fluorescence

intensity of liposomes was markedly higher in the lung after 48h (Fig. 7C). Additionally, similar results were obtained in the images of organ (Fig. 7D). Then a silica-induced pulmonary fibrosis model was established using the scheme illustrated in Fig. 7E, the mice were administered intravenously with Scrambled siRNA or NPM1 siRNA-loaded liposomes on day 8, day 15 and day 22 after silica treatment (Fig. 7E). Interestingly, histological evaluation with H&E staining, Masson's trichrome stain, and Sirius red consistently revealed the antifibrotic effects of NPM1 siRNA-loaded liposomes. The levels of collagen deposition and hydroxyproline in NPM1 siRNA-loaded liposomes-treated mice were lower than those in Scrambled siRNA-loaded liposomes mice (Fig. 7F and G). Consistently, mice administered NPM1 siRNA-loaded liposomes exhibited marked attenuation of fibrotic markers (Fibronectin, Collagen I, α-SMA) and NPM1 at the protein levels and mRNA levels (Fig. 7H, I, J and K). Collectively, our experiments suggested the potential clinical value of NPM1 siRNA-loaded liposomes administration in the treatment of silicosis.

Discussion

Silicosis is a non-reversible process characterized by chronic inflammation and progressive fibrosis, leading to a severe loss of lung function, poor quality of life, and early mortality [23]. A growing body of evidence suggests that the differentiation of pulmonary fibroblasts is the terminal effector process in silicosis. Upon repetitive injury, the alveolar epithelial basal membrane loses integrity, and interstitial (myo)fibroblasts migrate across the fenestrations in these membranes into the intra-alveolar masses to produce excessive ECM, which eventually leads to lung destruction and even respiratory failure [5]. Although silicosis exhibits a significant inflammatory response throughout the whole process of disease, published studies have demonstrated that once fibrosis has been established, anti-inflammatory therapy is not enough to postpone or reverse fibrosis [24]. Currently, lung transplantation is the only effective therapy for silicosis. Meanwhile, its highly limited availability, including the shortage of available donated organs and long-term postsurgical immunosuppression, determines that it cannot be broadly used [25]. Thus, identifying the factors that modulate fibroblast differentiation is of critical importance to further develop effective therapeutic strategies for silicosis. In the present study, evidence from pulmonary fibrosis models demonstrates that IL33 is a crucial factor involved in pulmonary fibrosis induced by BLM or silica treatment. We detected higher levels of IL33 in pulmonary fibrosis mice compared to the control groups. Mechanically, exogenous IL33 or IL33 secreted from silica-injured lung epithelial cells promoted the FMT by activating the ERK1/AP-1/NPM1 pathway via ST2, then exaggerated the development of silicosis. Further, treatment with NPM1 siRNA-loaded liposomes notably protected mice from silica-induced pulmonary fibrosis.

IL33 is usually localized in the nucleus and released into the extracellular environment in response to tissue injury, infectious agents, necrosis, necroptosis, and ferroptosis [11, 26]. As a damage-associated molecular pattern (DAMP) and alarmin, IL33 has various immunological effects and is thought to be one of the central cytokines involved in the innate immune and adaptive response [11]. Upon release, IL33 can stimulate a large number of immune cells such as mast cells (MCs), basophils, regulatory T-cells (Tregs), innate lymphoid cells (ILCs) and natural killer T cells (NKT), CD4 T cell subsets (Th1/2/17), CD8 T cells, and B cells, etc. [27]. It's well known that IL33 is involved in inflammatory processes. However, evidence

suggests IL33 also plays a role in wound healing and organ fibrosis. Data indicates that when acute and massive liver damage occurs, the release of IL33 by injured hepatocytes might act as an activator of tissue-protective mechanisms, while in chronic injury, IL33 plays the role of a hepatic fibrotic factor [28]. Epithelial-IL33 is also increased in pediatric Crohn's ileitis and is strongly associated with complicated fibrostenotic disease [29]. Apart from function as a biochemical marker of ischemia-reperfusion injury (IRI), IL33 can also mediate EMT of the renal tubular, which is a remarkable process in the pathogenesis of renal interstitial fibrosis [30]. In animal models, bleomycin enhances the production of IL33 in lung tissue and exerts a synergistic effect with IL33 on collagen accumulation, while deletion of ST2 attenuated the bleomycin-induced lung inflammation and fibrosis [31]. Our results also showed similar results. Notably, the protein levels of IL33 increased robustly in the IPF patients [32]. Thus, these findings support that IL33 acts as a candidate cytokine participating in the progression of fibrosis. In the present study, higher levels of IL33 were detected in lung tissues of pulmonary fibrosis mice, indicating that IL33 may be a potential contributor to the pathogenesis of silicosis.

Next, we focused on assessing lung cell lineages that can respond to IL33 during silicosis. M2 macrophages, known as the key participants of silicosis, can be polarized by IL33 to increase the production of IL13 and TGF-β, which are closely related to the activation of fibroblasts and ECM deposition [33]. In addition, IL33 can also stimulate the rapid expansion of ILCs, eosinophils, and MCs to produce IL13 and IL5 [34]. Current pathogenic theories demonstrate that FMT plays a central role in the pathogenesis of silicosis when fibroblasts are exposed to pro-fibrotic factors [35]. However, little information is known about the role of IL33 in fibroblasts. This inspired us to evaluate the direct impact of IL33 on fibroblasts. Our results suggested that exogenous IL33 promoted the activation of pulmonary fibroblasts in a dose-dependent manner. Silence of ST2, the specific receptor of IL33, significantly abolished the activation of fibroblasts induced by IL33 treatment.

The following issue was how IL33 promoted the FMT of fibroblasts via ST2. Binding of IL33 to ST2, with the presence of additional interleukin-1 receptor accessory protein (IL-1RacP) receptor protein molecules, results in activation of ERK, p38, JNK, NF-kB, phosphoinositide-3 kinase (PI3K) and the mTOR pathway signaling with various consequent effects in target cells [36]. ERK has been shown to regulate a variety of cellular functions, including cell growth, proliferation, differentiation, migration, and apoptosis [16]. Also, it's proved that ERK is activated in epithelial cells, macrophages, and fibroblasts in response to crystalline silica [37]. We, therefore, examined the effect of IL33 on ERK activation. Similar to previous studies, we found that IL33 promoted FMT progress in vitro by mediating the activation of p-ERK via ST2. Further, previous studies have shown that AP-1 intersects many signaling pathways as an ERK downstream target [38]. Since c-Jun is a major component of the AP-1 transactivator complex, it has been confirmed that hypoxia-induced release of preadipocyte factor-1 (Pref-1)- mediated CTGF expression via the α5β1 integrin receptor/ERK/c-Jun pathway in human lung fibroblasts may play a role in airway fibrosis in chronic obstructive asthma [39]. Besides, a study illustrated that resveratrol (Res) treatment blocked the activation of ERK/AP-1 pathways and suppressed miR-21 expression, which inhibited Smad7, subsequently leading to an alleviation of BLM-induced pulmonary fibrosis [40]. More importantly, the silica-activated ERK signaling pathway contributes to the cell cycle alteration by activating AP-1, thereby

promoting cell proliferation [41]. Indeed, high levels of AP-1 were observed in lung sections treated by silica and BLM, consistent with results demonstrated in vivo. Treatment with IL33 induced significant expression of AP-1 in pulmonary fibroblasts in a dose-dependent manner and could modulate the ERK/AP-1 pathway activation in fibroblasts via ST2. Although c-Fos was confirmed to act as a major regulator in tissue fibrosis and we also confirmed the elevated expression of c-Fos in fibrosis lung tissue, the levels of c-Fos induced by IL33 were unchanged after the knockdown of ST2 in MRC-5 in our study. These results suggested that the activated c-Fos may be regulated by other signalings, such as the NF-κB cascades [42]. Therefore, the following study is mainly focused on c-Jun, and the effect of c-Fos on pulmonary fibrosis still needs further exploration. Knockdown of c-Jun significantly abrogated the activation, proliferation, and migration of fibroblasts induced by IL33.

Given that AP-1 is a vital transcription factor and plays a critical role in the regulation of diverse downstream target genes such as fibrogenic, inflammatory, and cell proliferation genes. Recently exploration found that AP-1 can regulate NPM1 expression by directly binding to its promoter in the context of cancer [21]. Besides, the induction of transcriptional regulator c-Jun upregulated the transcriptional level of NPM1 in primary bone marrow stroma cells [19]. In the present study, we detected the expression of NPM1 in lung sections. Its expression was dramatically induced after BLM and silica treatment. Consistent with results demonstrated in vivo, treatment with IL33 increased the expression of NPM1 in pulmonary fibroblasts in a dose-dependent manner. ChIP assay together with c-Jun gain- and loss-of-function assay demonstrated that IL33 promoted the expression of NPM1 by potentiating ERK/AP-1 signaling in the pulmonary fibroblasts.

Injury and subsequent dysfunction of the lung epithelium are central to initiating the pathogenic process in silicosis. The mechanisms and mediators linking epithelial cell dysfunction to tissue fibrosis have not yet been comprehensively determined. Meanwhile, crosstalk between epithelial cells, immune cells, and nearby mesenchymal cell populations is central to this process [43]. As IL33 is recognized as epithelial alarmins, we then found that the markedly higher expression of IL33 was detected in epithelial cells after silica treatment. Epithelial-derived IL33 promoted the activation of pulmonary fibroblasts by potentiating the ERK/AP-1/NPM1 pathway via ST2 in the progression of silicosis.

It is suggested that direct targeting ERK may not be an effective therapeutic strategy for fibrosis as the signaling molecules exert multifunctional effects on various biological processes, including tissue homeostasis, cell proliferation and differentiation, and protein synthesis [44]. We assessed the treatment potential of targeting NPM1 in silica-induced pulmonary fibrosis mice. Previous studies demonstrated that cationic liposomes are promising strategies for the siRNA-based therapy of lung disease owing to their safety and ability to provide controlled drug release in the lung [45, 46]. The siRNA-loaded liposomes (patisiran) have been applied in clinical practice in 2018 [47]. Similarly, in the present study, NPM1 siRNA-loaded liposomes were efficiently distributed in lung tissue after intravenous injection. Excitingly, liposomes carrying NPM1 siRNA attenuated pulmonary fibrosis induced by silica, further suggesting the therapeutic potential of targeting NPM1.

However, this study has several limitations. First, further clinical cohort study would be helpful to verify the treatment efficiency of NPM1 siRNA-loaded liposomes. Second, although we illustrate that IL33 is derived from epithelial cells treated with silica, IL33-secreted from other types of cells and the mechanism of IL33 secretion needs further exploration. Third, the damaged alveolar epithelium can also produce other alarmins, including IL25 and thymic stromal lymphopoietin (TSLP). Whether these mediators participate in the progression of silicosis by modulating the cell-cell interaction require further verification.

Conclusions

In summary, the present study identified that the expression of NPM1 is elevated in mice with silicosis. Epithelial-derived IL33 releases and acts on pulmonary fibroblasts to potentiate the expression of NPM1 by activating the ERK1/AP-1 pathway via ST2 in silicosis. Treatment with NPM1 siRNA-loaded liposomes markedly protected mice from silica-induced pulmonary fibrosis in vivo. These data indicate that methods targeting NPM1 may have anti-fibrotic potential in silicosis treatment.

Material And Methods

Establishment of pulmonary fibrosis model induced by silica. Pulmonary fibrosis was induced in mice (C57BL/6 background) by intratracheal instillation with 50mg/kg of silica particles (size distribution: 99% between 0.5 and 10μm, 80% between 1 and 5μm, average particle diameter 1.7μm, obtained from SigmaAldrich, St. Louis, MO, USA) dissolved in 0.05 ml sterile saline. Mice administered the same volume of sterile saline served as controls. On days 8, 15 and 22 following the silica treatment, mice were intravenously injected with Scrambled siRNA or NPM1 siRNA-loaded liposomes. Finally, the mice were euthanized on days 28 after the silica treatment. The lung tissues were isolated and stored at – 80°C for further analysis.

Establishment of pulmonary fibrosis model induced by BLM. Pulmonary fibrosis was induced in mice (C57BL/6 background) by intratracheal instillation with 6 mg/kg BLM (Warbio, Nanjing, China) in 40 μl of sterile saline. Mice administered the same volume of sterile saline served as control subjects. Finally, the mice were euthanized on days 7, 14 and 21 following the BLM instillation, respectively. The lung tissues were isolated and stored at – 80°C for further analysis.

Pathological staining and histopathologic assessment. The mice lung tissues were harvested at 28 days after silica or saline administration, fixed with formalin solution overnight and embedded in paraffin. The tissue sections were then stained with hematoxylin and eosin (H&E), Masson’s trichrome stain and Sirius red.

Hydroxyproline assay. The amounts of lung collagen deposition were assessed by measuring the hydroxyproline content of lung tissue sections with a hydroxyproline assay kit (Jiancheng Bioengineering Institute, Nanjing, China). In accordance with the manufacturer’s protocol, the samples were determined by the spectrophotometer at 550 nm. The hydroxyproline concentration in the sample was calculated

from a standard curve and related to the amount of lung tissue used. The hydroxyproline contents in the lung tissues are given as μg of hydroxyproline per mg of lung tissue.

Cell culture and treatment. The human lung epithelial cells (BEAS-2B), human lung fibroblast (MRC-5) cells were commercially obtained from the American Type Culture Collection (ATCC, Manassas, VA, USA). BEAS-2B cells were maintained in Dulbecco's Modified Eagle Medium (DMEM, Life Technologies/Gibco, Grand Island, NY, USA), and the MRC-5 cells were maintained in Minimum Essential Medium (MEM, Life Technologies/Gibco, Grand Island, NY, USA). Primary mouse pulmonary fibroblasts (PMLFs) were isolated from the lung tissues of C57BL/6 mice. Briefly, fibroblasts were generated by mincing lung tissue into submillimeter-sized pieces, plated evenly in 60mm plates containing 4 ml of medium, which was changed after 24 h. Cells were cultured in Dulbecco's Modified Eagle Medium (DMEM, Life Technologies/Gibco, Grand Island, NY, USA).

All of the culture media were containing 10% fetal bovine serum (Biological Industries) and antibiotics (penicillin and streptomycin, Life Technologies/Gibco, Gaithersburg, MD). Cells were cultured at 37°C in a 5% CO_2 atmosphere. Epithelial cells were treated with 0, 50, 100, 150, 200, 250μg/ml Silicon dioxide (SiO_2) (Sigma-Aldrich, St. Louis, MO, USA); MRC-5 and PMLFs cells were treated with 0, 1, 2, 5 ng/ml exogenous IL33 (PeproTech) for 24h.

Cell transfection. Small interfering RNAs (siRNAs) specific for IL33, ST2, c-Jun, NPM1 were synthesized by Generay Biotech (Shanghai, China). Cells were transiently transfected using riboFECT CP Regent (RiboBio, Guangzhou, China) according to the manufacturer's instructions. Transfection efficiency was monitored by RT-PCR at 48 h after transfection. The sequence of human IL33: sense: GCUCUGGCCUUAUGAUAAATT; antisense: UUUAUCAUAAGGCCAGAGCTT.

The sequence of human ST2: sense: GGAUUGGUAUUACUCACAATT; antisense: UUGUGAGUAAUAACCAAUCCTT. The sequence of mouse ST2: sense: GGAAUGGUAUUACUCAGAUTT; antisense: AUCUGAGUAAUACCAUUCCTT. The sequence of human c-Jun: sense: GAAAGUCAUGAACCACGUUTT; antisense: AACGUGGUUCAUGACUUUCTT. The sequence of mouse c-Jun: sense: GCAAAGAUGGAAACGACCUTT; antisense: AGGUCGUUUCCAUCUUUGCTT. The sequence of human NPM1: sense: GAGCACCAGUUAUCUUUAATT; antisense: UUAAAGAUAACUGGUGCUCTT. The sequence of mouse NPM1 (#1): sense: CUAUCACUUUAAAGUGGAUTT; antisense: AUCCACUUUAAAGUGAUAGTT. The sequence of mouse NPM1 (#2): sense: CAGAAGCAAUGAACUAUGATT; antisense: UCAUAGUUAUUGCUUCUGTT. The sequence of mouse NPM1 (#3): sense: GACAGCAUCUAGUAGCUGUTT; antisense: ACAGCUACUAGAUGCUGUCTT.

c-Jun-plasmid and a vector plasmid were purchased from Generay Biotech (Shanghai, China), and 2μg of purified DNA was mixed with transfection reagent and applied to the cells. 48 h after transfection and co-transfection with IL33, the cells were analyzed by Western blot and RT-PCR.

Real-time PCR. Total RNA from collected tissues or cells was extracted using the Trizol reagent (Tiangen Biotech, Beijing, China). RNA quality and concentration were measured by Nanodrop 2000

spectrophotometer (Termo, Waltham, MA). All mRNA was detected using AceQ qPCR SYBR Green Master Mix (Vazyme Biotech Co, Nanjing, China) in the ABI 7900HT Real-Time PCR system (Applied Biosystems). Fold changes in the expression levels were calculated using the $2-\Delta\Delta Ct$ method and normalized using GAPDH as the endogenous control.

Western blot and antibodies. For western blot assay, all cells were washed twice times with PBS and then used with RIPA lysis buffer and phenylmethylsulfonyl fuoride for extraction of total proteins (Beyotime Institute of Biotechnology, Shanghai, China; PMSF, Sigma-Aldrich, St. Louis, MO, USA). The total protein of the mouse lung tissues was extracted with T-PER Tissue Protein Extraction Reagent (Termo Scientifc). Protein concentrations were measured by BCA Protein Assay (Beyotime Institute of Biotechnology, Shanghai, China). A total of 80 μg of protein extracts were separated via SDS-PAGE and transferred onto polyvinylidene difuoride (PVDF) membranes (ISEQ00010, 0.2 μm, Immobilon). Then the membranes were incubated overnight at 4°C with appropriate primary antibodies and appropriate secondary antibodies. Protein bands were visualized using the ChemiDocXRS + imaging system (Bio-Rad Laboratories, Inc). The gray values were analyzed with ImageJ software.

The primary antibodies used were anti-Fibronectin (Abcam); anti-Collagen I (ABclonal); anti-αSMA (Abcam); p-ERK (Cell Signaling Technology); ERK (Cell Signaling Technology); p-c-Jun (Cell Signaling Technology); c-Jun (Cell Signaling Technology); NPM1 (ABclonal); anti-GAPDH (ABclonal).

Cell proliferation assay. PMLFs were cultured in 96-well plates at a density of 2×10^3 cells/well. Cell proliferation was then measured using the EdU proliferation assay (Ribobio, Guangzhou, China), according to the manufacturers' instructions. Briefly, 18 h after being seeded in the plates, cells were labeled with EdU for 2h at 37°C, treated with 100μL of Apollo reaction cocktail and stained with 100μL of Hoechst 33342. Finally, the cells were observed under a fluorescence microscope (Olympus, Tokyo, Japan).

Cell viability assay. Cell viability was detected with a Cell Counting Kit-8 assay (CCK8, Beyotime Institute of Biotechnology, Shanghai, China) according to the manufacturer's instructions. The cells were plated in a 96-well plate, followed by exposure to different treatments for the indicated times. Then 10μl CCK8 reagents were diluted in each well for 1 h at 37°C in 5% CO_2, and the 96-well plate was measured at 450 nm carried out with a microplate reader (TECAN Infnite M200, Mannedorf, Switzerland).

Woundhealing assay. Cells were seeded in 6-well plates and cultured until the cells reached 70–80% confluence. Wounds were scratching with a sterile 200μl pipette tip across the monolayered cells to create a straight linear scratch, and a wound gap was performed by a microscope. After indicated treatment, the widths of the wound were followed by the previously described procedure. The wound gap was quantitatively evaluated with ImageJ software.

Immunostaining assay. Cryosections of lung tissues from mice with the onset of silica-induced pulmonary fibrosis were used for immuno-fluorescence staining. The primary antibodies used for staining were as follows: anti-αSMA (Abcam), anti-Collagen I (ABclonal), NPM1 (ABclonal), and Cy3-conjugated or

FITC-conjugated goat anti-rabbit antibody (Beyotime Institute of Biotechnology, Shanghai, China) were used as fluorescent secondary antibodies. Besides, after the indicated treatment, MRC-5 cells were washed fixed with 4% methanol for 30 min, then stained with anti-αSMA (Abcam) at 4°C overnight and incubated with Cy3-conjugated goat anti-rabbit antibody (Beyotime Institute of Biotechnology, Shanghai, China) for 1h. The DAPI was used to stain the nucleus in cells for 5 min. All the images were acquired with the fluorescence microscope (Olympus, Tokyo, Japan).

ChIP assay. The ChIP assay was performed to analyze the binding of c-Jun to the NPM1 promoter using a ChIP Assay Kit (CCK8, Beyotime Institute of Biotechnology, Shanghai, China) according to the manufacturer's instructions. Briefly, protein and DNA complex was precipitated with specific antibody against c-Jun (Cell Signaling Technology) and immunoglobulin G control (Millipore). Then, the purified DNA was suspended in Tris-EDTA buffer. PCR was performed to analyze the NPM1 promoter region.

Liposomes: Liposomes were raised as carriers to encapsulate siRNA. The lipid mixture including lipidoid, cholesterol, DSPC and mPEG-DMG dissolved in ethanol at a molar ratio of 50:38.5:10:1.5 were prepared. The unentrapped free siRNA was removed by ultrafiltration centrifugation. The hydrodynamic diameter, zeta potential and stability of the liposomes were measured by dynamic light scattering (DLS) (Malvern Zetasizer Nano-ZS, UK). After staining with 2% phosphotungstic acid, the liposomes were characterized by transmission electron microscopy (TEM, Jeol, Japan).

In vivo and ex vivo biodistribution of the liposomes. In vivo biodistribution of the liposomes, after si-NPM1 liposomes were constructed, the prepared liposomes were intravenous injection into the mice after 7 days of silica induction. Subsequently, the mice were anesthetized and photographed at different time points (0h, 24h, 48h) by an in vivo imaging system (IVIS Lumina XR, SI Imaging, AZ, USA). Similarly, the mice were euthanized and the organs were harvested for ex vivo fluorescence imaging, respectively.

Statistical analysis. All experiments were performed in triplicates calculated by GraphPad Prism (San Diego, CA, USA). Statistical analysis was performed using Student's t-test (between two groups) or one-way analyses of variance followed by Tukey's multiple comparisons test (more than two groups). Data were expressed as mean ± SD. $P < 0.05$ was considered statistically significant.

Declarations

Acknowledgments

Not applicable.

Author contributions

Y.W. and D.C. performed experiments and wrote the manuscript. Z.L. and W.S. performed experiments. L.P., H.X., and X.J. performed experiments. W.L., S.Z., and L.H. performed computational analysis. Y.L. designed the project and performed language editing. C.N. supervised experimental design and coordinated the study. All authors reviewed and approved the manuscript.

Funding

This project was supported by grants from the National Natural Science Foundation of China (82103804, 82073518), the Natural Science Foundation of Jiangsu Province (BK20210537), the Postdoctoral Research Supportive Project of Suzhou College of Nanjing Medical University 2021 (GSBSHKY202102).

Availability of data and materials

The datasets used and/or analyzed during the current study are available from

the corresponding author on reasonable request.

Ethics approval and consent to participate

All use of C57BL6 mice in this study were purchased from the Animal Center of Nanjing Medical University. All experimental procedures were carried out in accordance with human-animal care standards and the claim of the Nanjing Medical University Ethics Committee (Nanjing, China).

Consent for publication

Not applicable.

Competing interests

The authors declare no competing interests.

Author details

[1] Department of Occupational Medical and Environmental Health, Key Laboratory of Modern Toxicology of Ministry of Education, Center for Global Health, School of Public Health, Nanjing Medical University, Nanjing, 211166, China. [2] Institute of Occupational Disease Prevention, Jiangsu Provincial Center for Disease Control and Prevention, Nanjing 210028, China. [3] Gusu School, Nanjing Medical University, Nanjing, 211166, China.

References

1. Cavalin C, Lescoat A, Ballerie A, Belhomme N, Jégo P, Jouneau S, et al. Beyond silicosis, is the world failing on silica hazards? The Lancet Respiratory Medicine. 2019;7 8:649 – 50; doi: https://doi.org/10.1016/S2213-2600(19)30174-2. https://www.sciencedirect.com/science/article/pii/S2213260019301742.
2. Barnes H, Goh NSL, Leong TL, Hoy R. Silica-associated lung disease: An old-world exposure in modern industries. Respirol (Carlton Vic). 2019;24 12:1165–75. doi:10.1111/resp.13695.
3. Rose C, Heinzerling A, Patel K, Sack C, Wolff J, Zell-Baran L, et al. Severe Silicosis in Engineered Stone Fabrication Workers - California, Colorado, Texas, and Washington, 2017–2019. MMWR

Morbidity and mortality weekly report. 2019;68 38:813–8; doi: 10.15585/mmwr.mm6838a1.

4. Adamcakova J, Mokra D. New Insights into Pathomechanisms and Treatment Possibilities for Lung Silicosis. Int J Mol Sci. 2021;22:8. doi:10.3390/ijms22084162.
5. Pang X, Shao L, Nie X, Yan H, Li C, Yeo AJ, et al. Emodin attenuates silica-induced lung injury by inhibition of inflammation, apoptosis and epithelial-mesenchymal transition. Int Immunopharmacol. 2021;91:107277. doi:10.1016/j.intimp.2020.107277.
6. Blanco-Pérez JJ, Blanco-Dorado S, Rodríguez-García J, Gonzalez-Bello ME, Salgado-Barreira Á, Caldera-Díaz AC, et al. Serum levels of inflammatory mediators as prognostic biomarker in silica exposed workers. Sci Rep. 2021;11 1:13348; doi:10.1038/s41598-021-92587-0.
7. Jiao J, Li L, Yao W, Qin W, Hao C, Lu L. Influence of Silica Exposure for Lung Silicosis Rat. Dis Markers. 2021;2021:6268091. doi:10.1155/2021/6268091.
8. Takenouchi Y, Kitakaze K, Tsuboi K, Okamoto Y. Growth differentiation factor 15 facilitates lung fibrosis by activating macrophages and fibroblasts. Exp Cell Res. 2020;391 2:112010. doi:10.1016/j.yexcr.2020.112010.
9. Lin S, Zhang R, Xu L, Ma R, Xu L, Zhu L, et al. LncRNA Hoxaas3 promotes lung fibroblast activation and fibrosis by targeting miR-450b-5p to regulate Runx1. Cell death & disease. 2020;11 8:706; doi: 10.1038/s41419-020-02889-w.
10. Chan BCL, Lam CWK, Tam LS, Wong CK. IL33: Roles in Allergic Inflammation and Therapeutic Perspectives. Front Immunol. 2019;10:364. doi:10.3389/fimmu.2019.00364.
11. Saikumar Jayalatha AK, Hesse L, Ketelaar ME, Koppelman GH, Nawijn MC. The central role of IL-33/IL-1RL1 pathway in asthma: From pathogenesis to intervention. Pharmacol Ther. 2021;225:107847. doi:10.1016/j.pharmthera.2021.107847.
12. Zizzo G, Cohen PL. Imperfect storm: is interleukin-33 the Achilles heel of COVID-19? The Lancet Rheumatology. 2020;2 12:e779-e90; doi: 10.1016/s2665-9913(20)30340-4.
13. Griesenauer B, Paczesny S. The ST2/IL-33 Axis in Immune Cells during Inflammatory Diseases. Front Immunol. 2017;8:475. doi:10.3389/fimmu.2017.00475.
14. Kotsiou OS, Gourgoulianis KI, Zarogiannis SG. IL-33/ST2 Axis in Organ Fibrosis. Front Immunol. 2018;9:2432. doi:10.3389/fimmu.2018.02432.
15. Barbosa R, Acevedo LA, Marmorstein R. The MEK/ERK Network as a Therapeutic Target in Human Cancer. Mol cancer research: MCR. 2021;19 3:361–74. doi:10.1158/1541-7786.Mcr-20-0687.
16. Xie Y, Ma J, Yang M, Fan L, Chen W. Extracellular signal-regulated kinase signaling pathway and silicosis. Toxicol Res. 2021;10 3:487–94. doi:10.1093/toxres/tfaa109.
17. Karimi Dermani F, Gholamzadeh Khoei S, Afshar S, Amini R. The potential role of nucleophosmin (NPM1) in the development of cancer. J Cell Physiol. 2021;236 11:7832–52. doi:10.1002/jcp.30406.
18. Peng HH, Ko HH, Chi NC, Wang YP, Lee HC, Pan PY, et al. Upregulated NPM1 is an independent biomarker to predict progression and prognosis of oral squamous cell carcinomas in Taiwan. Head Neck. 2020;42 1:5–13. doi:10.1002/hed.25971.

19. Wernig G, Chen SY, Cui L, Van Neste C, Tsai JM, Kambham N, et al. Unifying mechanism for different fibrotic diseases. Proc Natl Acad Sci USA. 2017;114 18:4757–62. doi:10.1073/pnas.1621375114.
20. Li Y, Zeng N, Qin Z, Chen Y, Lu Q, Cheng Y, et al. Ultrasmall Prussian blue nanoparticles attenuate UVA-induced cellular senescence in human dermal fibroblasts via inhibiting the ERK/AP-1 pathway. Nanoscale. 2021;13 38:16104–12. doi:10.1039/d1nr04268h.
21. Senapati P, Dey S, Sudarshan D, Das S, Kumar M, Kaypee S, et al. Oncogene c-fos and mutant R175H p53 regulate expression of Nucleophosmin implicating cancer manifestation. FEBS J. 2018;285 18:3503–24. doi:10.1111/febs.14625.
22. De Giacomi F, Vassallo R, Yi ES, Ryu JH. Acute Eosinophilic Pneumonia. Causes, Diagnosis, and Management. Am J Respir Crit Care Med. 2018;197 6:728–36. doi:10.1164/rccm.201710-1967CI.
23. Wollin L, Distler JHW, Redente EF, Riches DWH, Stowasser S, Schlenker-Herceg R, et al. Potential of nintedanib in treatment of progressive fibrosing interstitial lung diseases. Eur respiratory J 2019;54 3; doi:10.1183/13993003.00161-2019.
24. Lenti MV, Di Sabatino A. Intestinal fibrosis. Molecular aspects of medicine. 2019;65:100–9; doi: 10.1016/j.mam.2018.10.003.
25. George PM, Patterson CM, Reed AK, Thillai M. Lung transplantation for idiopathic pulmonary fibrosis. The Lancet Respiratory medicine. 2019;7 3:271–82. doi:10.1016/s2213-2600(18)30502-2.
26. Chen C, Wang D, Yu Y, Zhao T, Min N, Wu Y, et al. Legumain promotes tubular ferroptosis by facilitating chaperone-mediated autophagy of GPX4 in AKI. Cell Death Dis. 2021;12 1:65; doi:10.1038/s41419-020-03362-4.
27. Eissmann MF, Buchert M, Ernst M. IL33 and Mast Cells-The Key Regulators of Immune Responses in Gastrointestinal Cancers? Frontiers in immunology. 2020;11:1389; doi: 10.3389/fimmu.2020.01389.
28. He Y, Hwang S, Ahmed YA, Feng D, Li N, Ribeiro M, et al. Immunopathobiology and therapeutic targets related to cytokines in liver diseases. Cell Mol Immunol. 2021;18(1):18–37. doi:10.1038/s41423-020-00580-w.
29. Masterson JC, Capocelli KE, Hosford L, Biette K, McNamee EN, de Zoeten EF, et al. Eosinophils and IL-33 Perpetuate Chronic Inflammation and Fibrosis in a Pediatric Population with Stricturing Crohn's Ileitis. Inflamm Bowel Dis. 2015;21 10:2429–40. doi:10.1097/mib.0000000000000512.
30. Zhu F, Bai X, Hong Q, Cui S, Wang X, Xiao F, et al. STAT3 Inhibition Partly Abolishes IL-33-Induced Bone Marrow-Derived Monocyte Phenotypic Transition into Fibroblast Precursor and Alleviates Experimental Renal Interstitial Fibrosis. Journal of immunology (Baltimore, Md: 1950). 2019;203 10:2644-54; doi: 10.4049/jimmunol.1801273.
31. Li D, Guabiraba R, Besnard AG, Komai-Koma M, Jabir MS, Zhang L, et al. IL-33 promotes ST2-dependent lung fibrosis by the induction of alternatively activated macrophages and innate lymphoid cells in mice. J Allergy Clin Immunol. 2014;134(6):1422–32.e11. doi:10.1016/j.jaci.2014.05.011.
32. Lee JU, Chang HS, Lee HJ, Jung CA, Bae DJ, Song HJ, et al. Upregulation of interleukin-33 and thymic stromal lymphopoietin levels in the lungs of idiopathic pulmonary fibrosis. BMC Pulm Med. 2017;17 1:39; doi:10.1186/s12890-017-0380-z.

33. Xiong Y, Cui X, Zhou Y, Chai G, Jiang X, Ge G, et al. Dehydrocostus lactone inhibits BLM-induced pulmonary fibrosis and inflammation in mice via the JNK and p38 MAPK-mediated NF-κB signaling pathways. Int Immunopharmacol. 2021;98:107780. doi:10.1016/j.intimp.2021.107780.
34. Nagashima R, Iyoda M. The Roles of Kidney-Resident ILC2 in Renal Inflammation and Fibrosis. Front Immunol. 2021;12:688647. doi:10.3389/fimmu.2021.688647.
35. Liu P, Miao K, Zhang L, Mou Y, Xu Y, Xiong W, et al. Curdione ameliorates bleomycin-induced pulmonary fibrosis by repressing TGF-β-induced fibroblast to myofibroblast differentiation. Respir Res. 2020;21 1:58; doi:10.1186/s12931-020-1300-y.
36. Homsak E, Gruson D. Soluble ST2: A complex and diverse role in several diseases. Clinica chimica acta; international journal of clinical chemistry. 2020;507:75–87; doi: 10.1016/j.cca.2020.04.011.
37. Nakashima K, Sato T, Shigemori S, Shimosato T, Shinkai M, Kaneko T. Regulatory role of heme oxygenase-1 in silica-induced lung injury. Respir Res. 2018;19 1:144; doi:10.1186/s12931-018-0852-6.
38. Kamata Y, Tominaga M, Umehara Y, Honda K, Kamo A, Moniaga CS, et al. Calcium-Inducible MAPK/AP-1 Signaling Drives Semaphorin 3A Expression in Normal Human Epidermal Keratinocytes. J Invest Dermatol. 2020;140 7(e5):1346–54. doi:10.1016/j.jid.2020.01.001.
39. Cheng WH, Lee KY, Yu MC, Chen JY, Lin CH, Chen BC. Pref-1 induced lung fibroblast differentiation by hypoxia through integrin α5β1/ERK/AP-1 cascade. Eur J Pharmacol. 2021;909:174385. doi:10.1016/j.ejphar.2021.174385.
40. Wang J, He F, Chen L, Li Q, Jin S, Zheng H, et al. Resveratrol inhibits pulmonary fibrosis by regulating miR-21 through MAPK/AP-1 pathways. Biomed pharmacotherapy = Biomedecine pharmacotherapie. 2018;105:37–44. doi:10.1016/j.biopha.2018.05.104.
41. Wang H, Xiao S, Tang Y, Han K, Zhang Z, Jin Y, et al. Activation of MAPK and Cyclin D1/CDK4 in Malignant Transformation of Human Embryonic Lung Fibroblasts Induced by Silica and Benzopyrene. Asian Pac J cancer prevention: APJCP. 2020;21 2:295–300. doi:10.31557/apjcp.2020.21.2.295.
42. Ariyoshi W, Okinaga T, Chaweewannakorn W, Akifusa S, Nisihara T. Mechanisms involved in enhancement of matrix metalloproteinase-9 expression in macrophages by interleukin-33. J Cell Physiol. 2017;232 12:3481–95. doi:10.1002/jcp.25809.
43. Wang Y, Li S, Zhao J, Li Q, Xu C, Wu H, et al. Snail-mediated partial epithelial mesenchymal transition augments the differentiation of local lung myofibroblast. Chemosphere. 2021;267:128870. doi:10.1016/j.chemosphere.2020.128870.
44. Sugiura R, Satoh R, Takasaki T. ERK: A Double-Edged Sword in Cancer. ERK-Dependent Apoptosis as a Potential Therapeutic Strategy for Cancer. Cells. 2021;10:10. doi:10.3390/cells10102509.
45. Wang Q, Liu J, Hu Y, Pan T, Xu Y, Yu J, et al. Local administration of liposomal-based Srpx2 gene therapy reverses pulmonary fibrosis by blockading fibroblast-to-myofibroblast transition. Theranostics. 2021;11 14:7110–25. doi:10.7150/thno.61085.

46. Wu X, Shu L, Zhang Z, Li J, Zong J, Cheong LY, et al. Adipocyte Fatty Acid Binding Protein Promotes the Onset and Progression of Liver Fibrosis via Mediating the Crosstalk between Liver Sinusoidal Endothelial Cells and Hepatic Stellate Cells. Advanced science (Weinheim, Baden-Wurttemberg, Germany). 2021;811:e2003721; doi: 10.1002/advs.202003721.
47. Zhang Y, Sun C, Wang C, Jankovic KE, Dong Y. Lipids and Lipid Derivatives for RNA Delivery. Chem Rev. 2021;121 20:12181–277. doi:10.1021/acs.chemrev.1c00244.

Figures

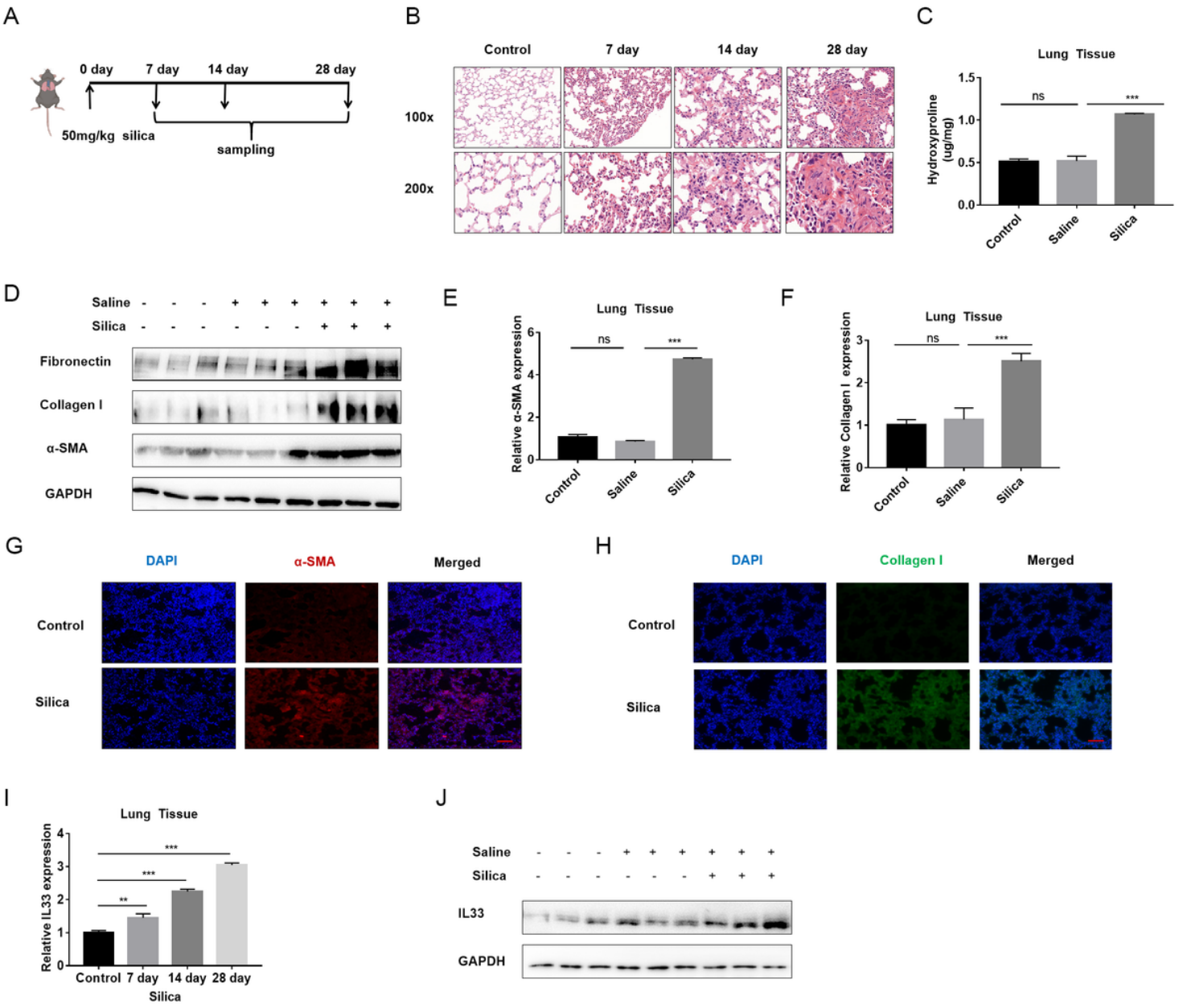

Figure 1

IL33 is overexpressed in silica-induced pulmonary fibrosis in vivo. **A** Schematic diagram of the experimental design and time course of silica-treated mice. **B** H&E staining reflected the histological changes of mice lung tissues after silica induction at different time points. **C** Quantifying hydroxyproline in mice induced by silica or saline for 28 days. Three mice were included in each study group, with ***p < 0.001 vs. saline group and ns, no signifcance vs. control group. **D**Western blot analysis of Fibronectin, Collagen I, and α-SMA expression in the lung tissues of mice induced by silica or saline for 28 days. **E, F** RT-PCR analysis of α-SMA and Collagen I expression, with ***p < 0.001 vs. saline group and ns, no signifcance vs. control group. **G, H** Immunofluorescence staining of α-SMA and Collagen I in the 28-day lung tissues from control and silica-induced mice. The nuclei were stained blue by DAPI, α-SMA stained red, and Collagen I stained green, scale bar=50μm. **I** RT-PCR analysis of IL33 expression in the lung tissues of mice induced by silica in different timepoints, with **p < 0.01, ***p < 0.001 vs. control group. **J** Western blot analysis of IL33 expression in the lung tissues of mice induced by silica or saline for 28 days.

Fig 1D and 1J were cut from the original blot images, see Additionnal File 2 for details.

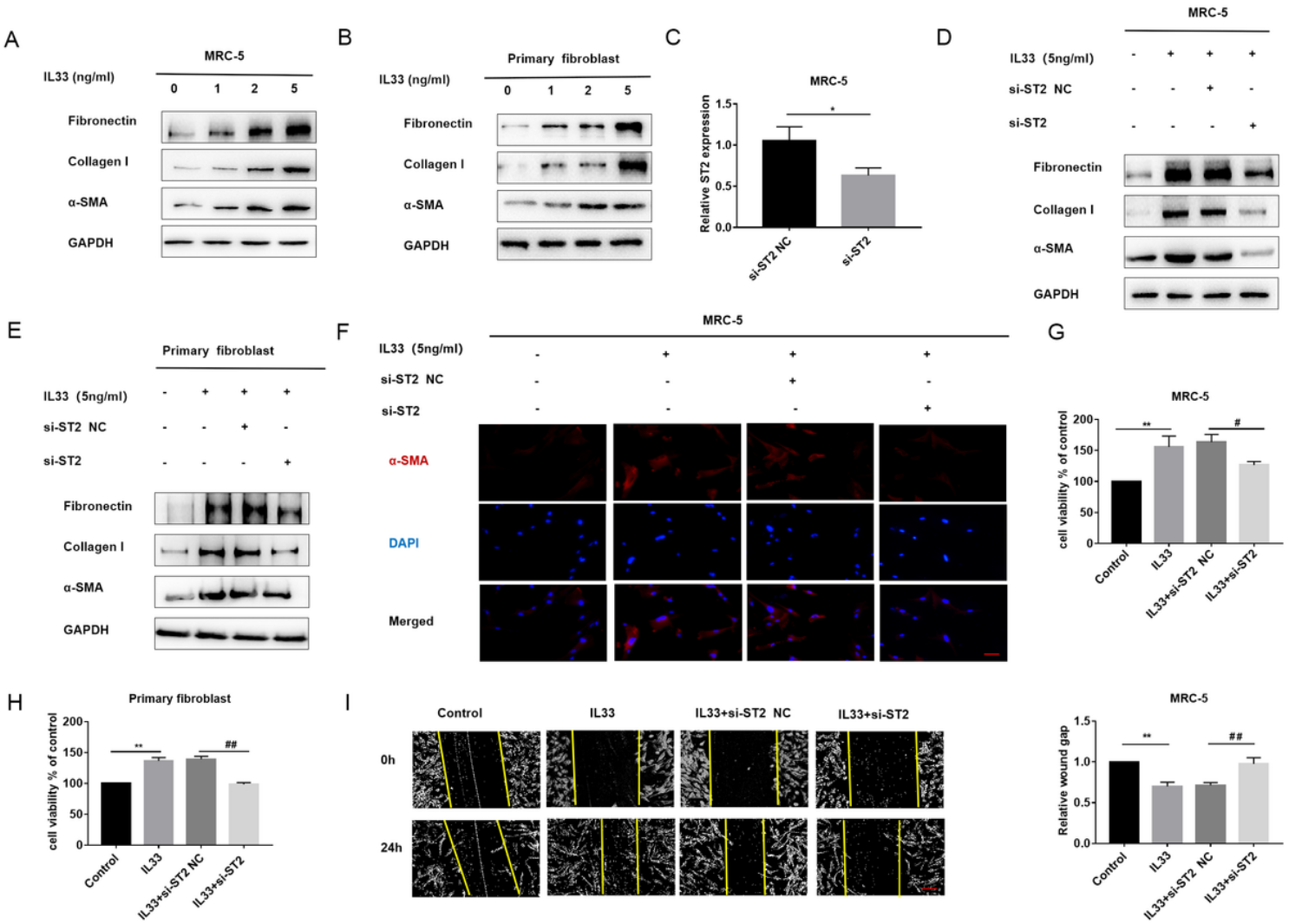

Figure 2

IL33 promotes the activation, proliferation and migration of pulmonary fibroblasts via ST2. **A, B** Western blot analysis of Fibronectin, Collagen I and α-SMA expression in MRC-5 cells and PMLFs treated with different doses of exogenous IL33 for 24 hours. **C** RT-PCR analysis of the interfering efficiency of ST2 siRNAs in MRC-5 cells, with *p<0.05 vs. si-ST2 NC group. **D, E**Western blot analysis of Fibronectin, Collagen I and α-SMA expression in si-ST2 or si-ST2 NC transfected MRC-5 cells and PMLFs following IL33 induction. **F**Immunofluorescence staining of α-SMA in si-ST2 or si-ST2 NC transfected MRC-5 cells following IL33 induction. The nuclei were stained blue by DAPI, α-SMA stained red, scale bar=50μm. **G, H** Cell viability was detected by CCK8 assay in MRC-5 cells and PMLFs. MRC-5 cells and PMLFswere transfected with si-ST2 or si-ST2 NC following IL33 induction, with **p<0.01 vs. control and #p<0.05, ##p<0.01 vs. IL33 plus si-ST2 NC group. **I** Wound-healing assay and quantifed wound gap of cell scratches detected the migration of MRC-5 cells. MRC-5 cells were transfected with si-ST2 or si-ST2 NC following IL33 induction, with **p<0.01 vs. control and ##p<0.01 vs. IL33 plus si-ST2 NC group, scale bar=50μm.

Fig 2A, 2B, 2D and 2E were cut from the original blot images, see Additionnal File 2 for details.

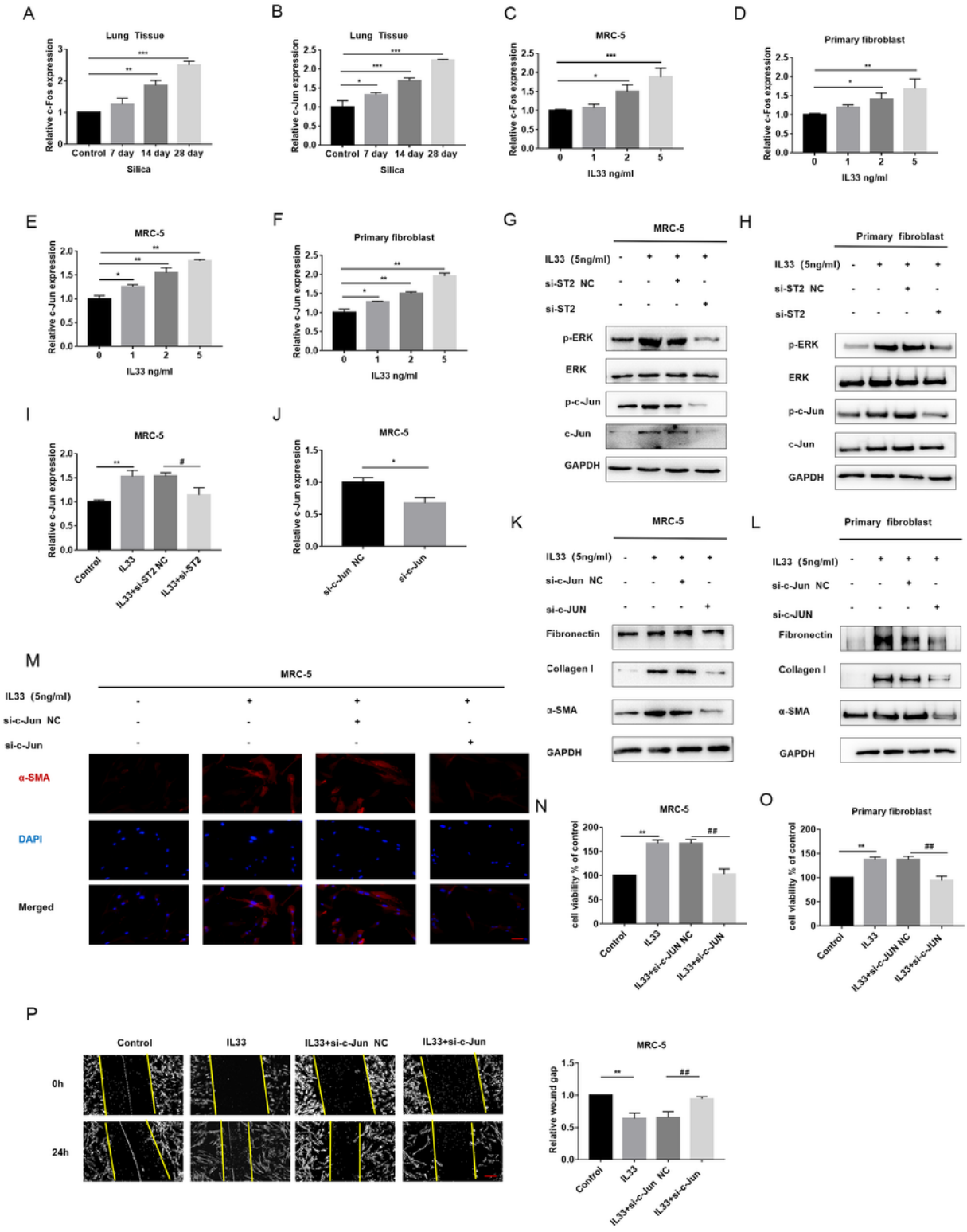

Figure 3

IL33 stimulates the activation, proliferation and migration of pulmonary fibroblasts by activating the ERK/AP-1 cascade via ST2. **A, B** RT-PCR analysis of c-Fos and c-Jun expression in the lung tissues of mice induced by silica in different timepoints, with *p < 0.05, **p < 0.01, ***p < 0.001 vs. control group. **C, D, E, F** RT-PCR analysis of c-Fos and c-Jun expression in MRC-5 cells and PMLFs treated with different doses of exogenous IL33 for 24 hours, with *p < 0.05, **p < 0.01, ***p < 0.001 vs. control group. **G, H**

Western blot analysis of the activation of ERK and c-Jun in si-ST2 or si-ST2 NC transfected MRC-5 cells and PMLFs following IL33 induction. **I** RT-PCR analysis of c-Jun expression in si-ST2 or si-ST2 NC transfected MRC-5 following IL33 induction, with **p < 0.01 vs. control group and #p<0.05 vs. IL33 plus si-ST2 NC group. **J** RT-PCR analysis of the interfering efficiency of c-Jun siRNAs in MRC-5 cells, with *p<0.05 vs. si-c-Jun NC group. **K, L**Western blot analysis of Fibronectin, Collagen I and α-SMA expression in si-c-Jun or si-c-Jun NC transfected MRC-5 cells and PMLFs following IL33 induction. **M** Immunofluorescence staining of α-SMA in si-c-Jun or si-c-Jun NC transfected MRC-5 cells following IL33 induction. The nuclei were stained blue by DAPI, α-SMA stained red, scale bar=50μm. **N, O** Cell viability was detected by CCK8 assay in MRC-5 cells and PMLFs. Cells were transfected with si-c-Jun or si-c-Jun NC following IL33 induction, with **p<0.01 vs. control and ##p<0.01 vs. IL33 plus si-ST2 NC group. **P** Wound-healing assay and quantified wound gap of cell scratches detected the migration of MRC-5 cells. Cells were transfected with si-c-Jun or si-c-Jun NC following IL33 induction, with **p<0.01 vs. control and ##p<0.01 vs. IL33 plus si-c-Jun NC group, scale bar=50μm.

Fig 3G, 3H, 3K and 3L were cut from the original blot images, see Additionnal File 2 for details.

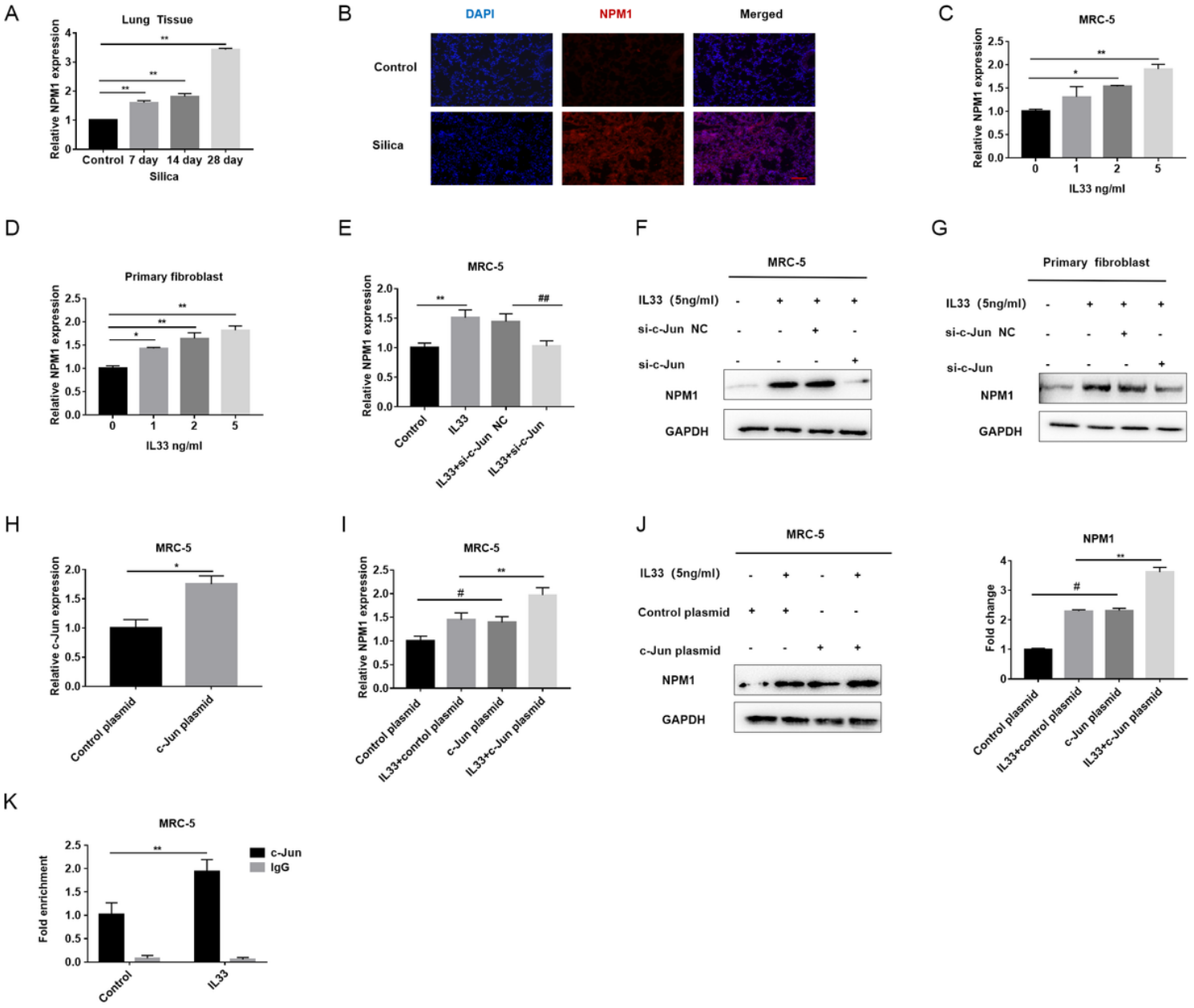

Figure 4

IL33 stimulates the expression of NPM1 in pulmonary fibroblasts by transcription factor AP-1. **A** RT-PCR analysis of NPM1 expression in the lung tissues of mice induced by silica in different timepoints, with **p < 0.01 vs. control group. **B** Immunofluorescence staining of and NPM1 in the 28-day lung tissues from control and silica-induced mice. The nuclei were stained blue by DAPI, NPM1 stained red, scale bar=50μm. **C, D** RT-PCR analysis of NPM1 expression in MRC-5 cells and PMLFs treated with different doses of exogenous IL33 for 24 hours, with *p < 0.05, **p < 0.01 vs. control group. **E, F, G** RT-PCR and Western blot analysis of NPM1 expression in si-c-Jun or si-c-Jun NC transfected MRC-5 and PMLFs following IL33 induction, with **p < 0.01 vs. control group and ##p<0.01 vs. IL33 plus si-c-Jun NC group. **H** RT-PCR analysis of the overexpression efficiency of c-Jun siRNAs in MRC-5 cells, with *p < 0.05 vs. control plasmid group. **I, J** RT-PCR and Western blot analysis of NPM1 expression in c-Jun plasmid or control plasmid transfected PMLFs following IL33 induction, with **p < 0.01 vs. IL33 plus control plasmid

group, #p<0.05 vs. control plasmid group. **K** ChIP assay was performed to analyze the binding of c-Jun to the NPM1 promoter following IL33 induction. Rabbit IgG was used as a control, with **p < 0.01 vs. control group.

Fig 4F, 4G and 4J were cut from the original blot images, see Additionnal File 2 for details.

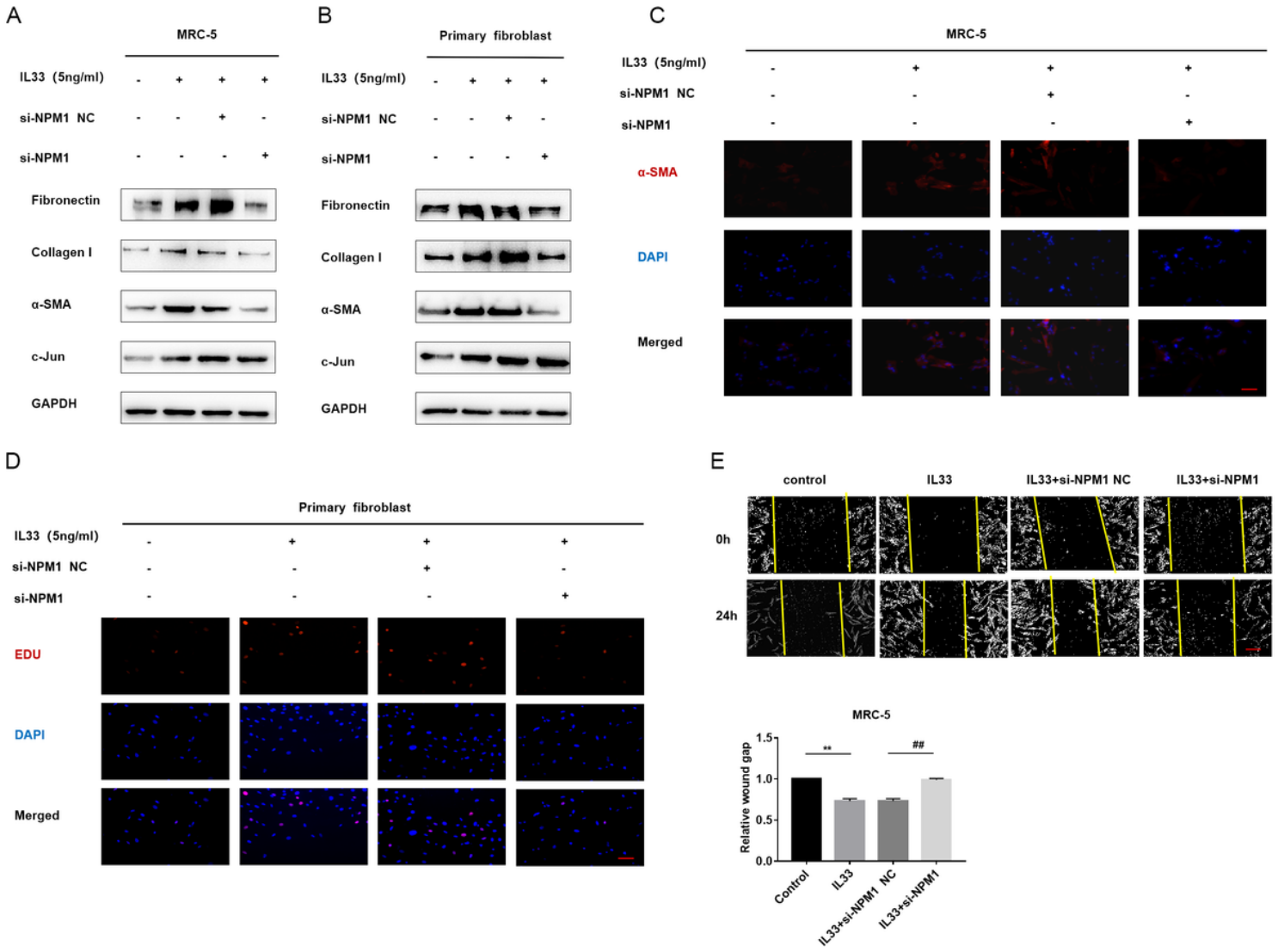

Figure 5

IL33 stimulates the activation, proliferation and migration of pulmonary fibroblasts by activating the ERK/AP-1/NPM1 cascade via ST2. **A, B** Western blot analysis of Fibronectin, Collagen I, α-SMA and c-Jun expression in si-NPM1 or si-NPM1 NC transfected MRC-5 cells and PMLFs following IL33 induction. **C** Immunofluorescence staining of α-SMA in si-NPM1 or si-NPM1 NC transfected MRC-5 cells following IL33 induction. The nuclei were stained blue by DAPI, α-SMA stained red, scale bar=50μm. **D** EdU staining in si-NPM1 or si-NPM1 NC transfected PMLFs following IL33 induction, scale bar=50μm. **E** Wound-healing assay and quantifed wound gap of cell scratches detected the migration of MRC-5 cells. MRC-5 cells were transfected with si-NPM1 or si-NPM1 NC following IL33 induction, with **p<0.01 vs. control and ##p<0.01 vs. IL33 plus si-NPM1 NC group, scale bar=50μm.

Fig 5 A and 5B were cut from the original blot images, see Additionnal File 2 for details.

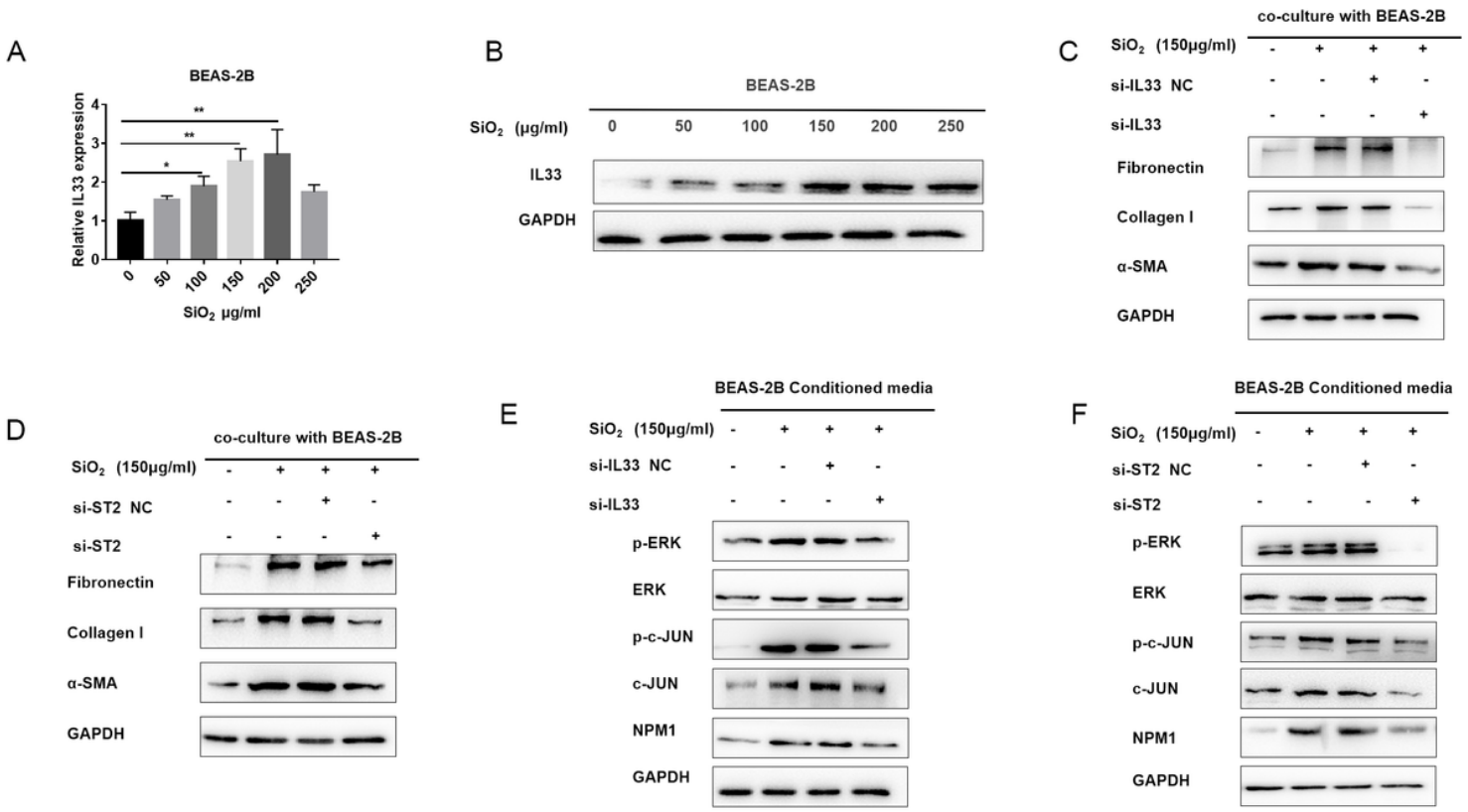

Figure 6

Epithelial-derived IL33 promotes the activation of pulmonary fibroblasts by potentiating the ERK1/AP-1/NPM1 pathway via ST2 in silicosis. **A, B** RT-PCR and Western blot analysis of IL33 expression in BEAS-2B cell with different doses of silica for 24 hours, with *p < 0.05, **p < 0.01 vs. control group. **C** Western blot analysis of Fibronectin, Collagen I, and α-SMA expression in MRC-5 cells co-cultured with BEAS-2B cells; BEAS-2B cells were treated with silica alone, or transfected with si-IL33 or si-IL33 NC following silica stimulation. **D** Western blot analysis of Fibronectin, Collagen I, and α-SMA expression in MRC-5 cells co-cultured with BEAS-2B cells; BEAS-2B cells were only induced by silica, MRC-5 cells were transfected with si-ST2 or si-ST2 NC. **E** Western blot analysis of the activation of ERK/AP-1 and NPM1 expression in MRC-5 cells treated with BEAS-2Bcells supernatants; BEAS-2B cells were treated with silica alone, or transfected with si-IL33 or si-IL33 NC following silica stimulation. **F**Western blot analysis of the activation of ERK/AP-1 and NPM1 expression in MRC-5 cells treated with BEAS-2B cells supernatants; BEAS-2B cells were only induced by silica, MRC-5 cells were transfected with si-ST2 or si-ST2 NC.

Fig 6B, 6C, 6D, 6E and 6F were cut from the original blot images, see Additionnal File 2 for details.

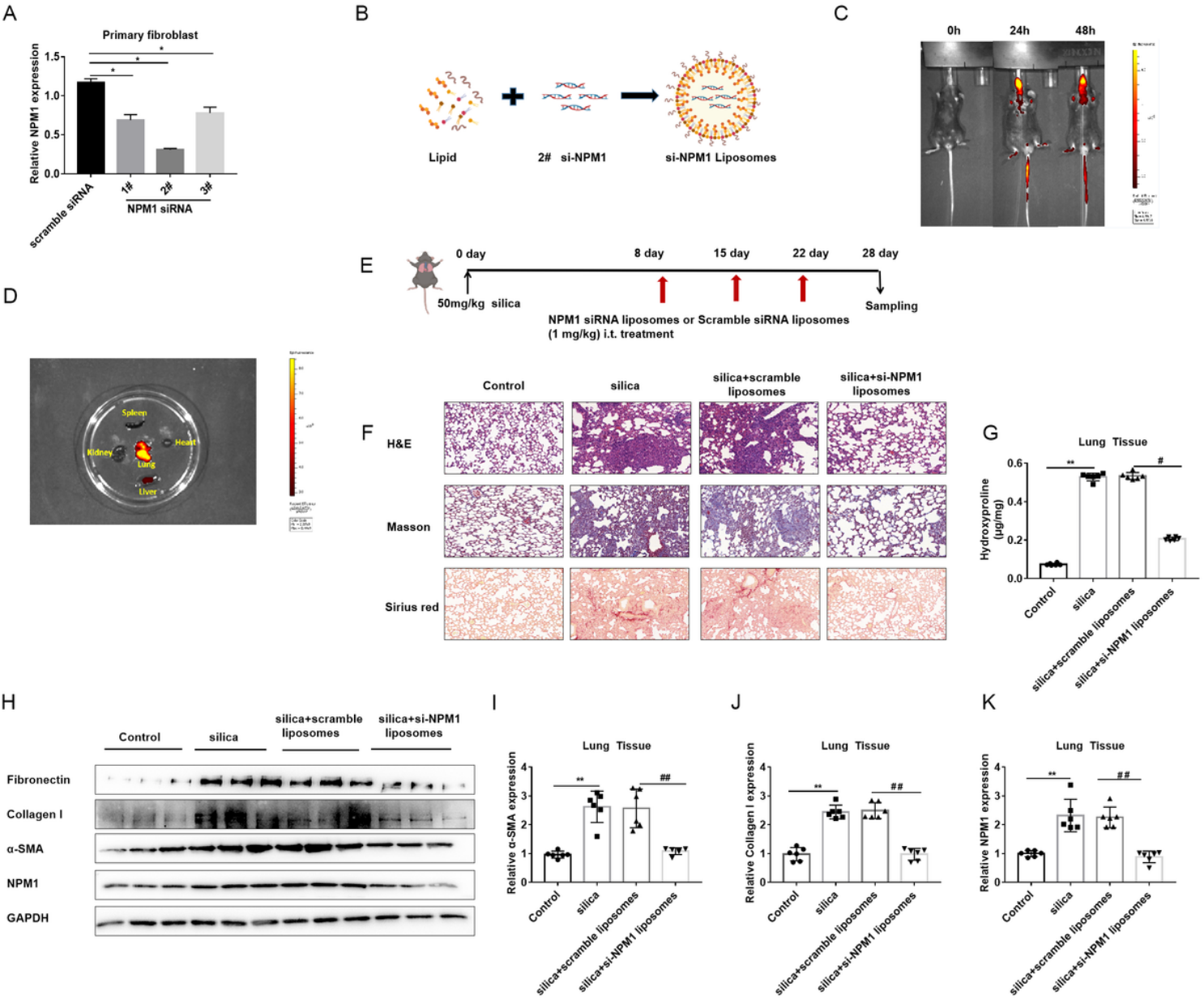

Figure 7

Treatment with liposomes carrying NPM1 siRNA evokes an anti-fibrotic response in silica-induced pulmonary fibrosis. **A** RT-PCR analysis of the interfering efficiency of NPM1 siRNAs in PMLFs,with *p < 0.05 vs. scramble siRNA group. **B** Schematic diagram for preparation of liposomes carrying NPM1 siRNA. **C, D** The biodistribution of the liposomes in silica-induced pulmonary fibrosis mice in vivo and ex vivo images. **E** Schematic diagram of the NPM1 siRNA-loaded liposomes treatment mouse model. **F** Histological analysis of the severity of lung fibrosis in mice after NPM1siRNA-loaded liposomestreatment. **G** Quantification of hydroxyproline in mice treated by NPM1 siRNA-loaded liposomes, with **p < 0.01 vs. control and #p<0.05 vs. silica plus scramble siRNA group. **H, I, J, K** Western blot and RT-PCR analysis of Fibronectin, Collagen I, α-SMA expression and NPM1 in lung tissues treated by NPM1siRNA-loaded liposomes, with **p < 0.01 vs. control and ##p<0.01 vs. silica plus scramble siRNA group.

Fig 7H were cut from the original blot images, see Additionnal File 2 for details.

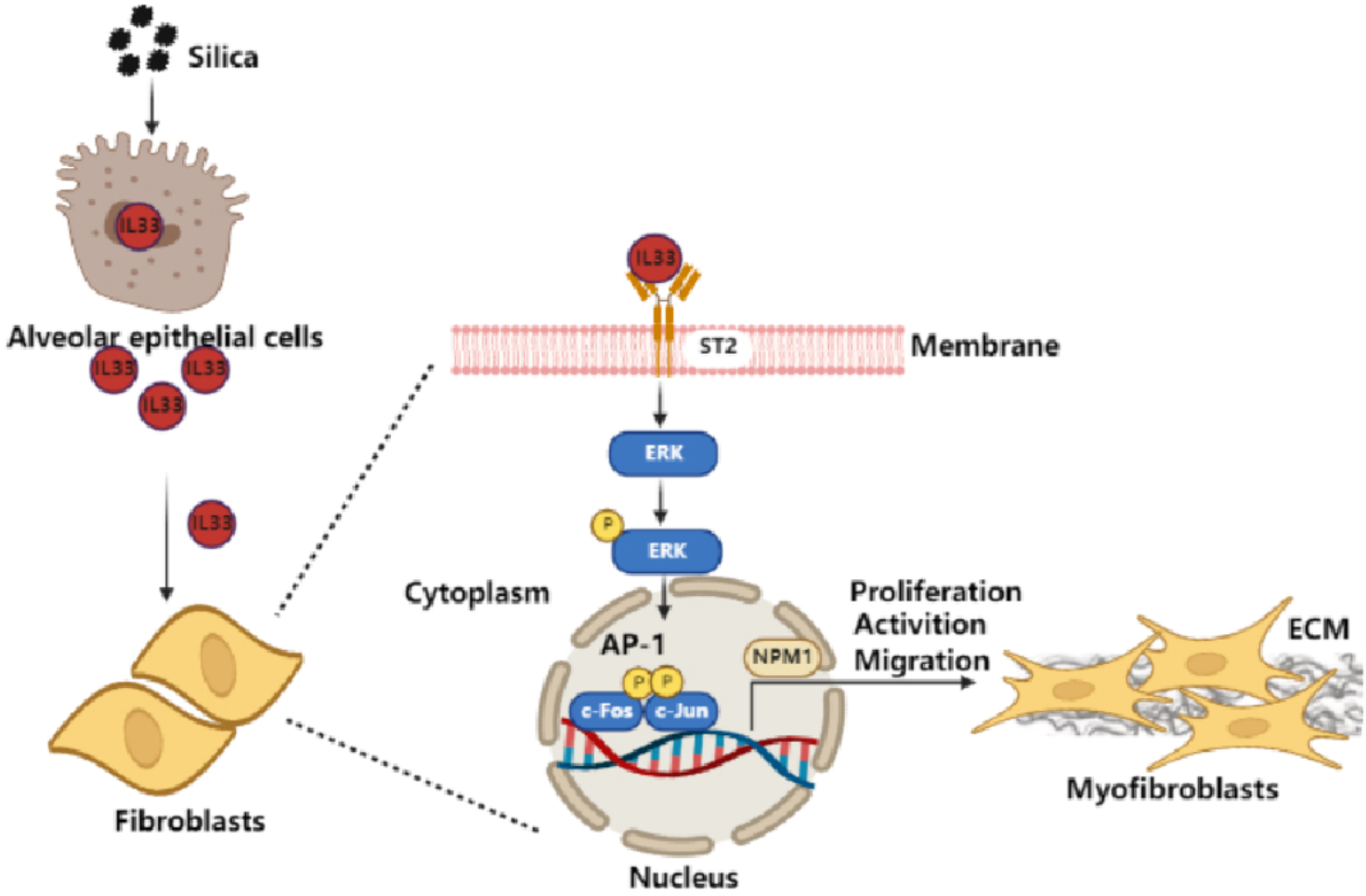

Figure 8

Schematic diagram illustrating the mechanism whereby IL33-mediated NPM1 expression involving in the process of silicosis. IL33 is secreted from damaged alveolar epithelial cells induced by silica, and then IL33 specially binds to ST2 and stimulates the expression of NPM1 through activating the ERK/AP-1 signaling, by which it facilitates the activation, proliferation and migration of pulmonary fibroblasts and extracellular matrix synthesis, therefore exaggerating silica-induced pulmonary fibrosis.

Supplementary Files

This is a list of supplementary files associated with this preprint. Click to download.

- Additionalfile1.docx
- Additionalfile2.pptx